

## Application of magnetic activated carbon coated with CuS nanoparticles as a new adsorbent for the removal of tetracycline antibiotic from aqueous solutions (isotherm, kinetic and thermodynamic study)

Narjes Sadat Mazari Moghaddam<sup>a</sup>, Behnam Barikbin<sup>b</sup>, Ethar M. Al-Essa<sup>c</sup>,  
Rasoul Khosravi<sup>d</sup>, Tariq Al-Musawi<sup>e</sup>, Negin Nasseh<sup>f,\*</sup>

<sup>a</sup>Environmental Health Engineering, Birjand University of Medical Sciences, Birjand, Iran,  
email: narjes\_moghaddam1995@yahoo.com

<sup>b</sup>Department of Environmental Health Engineering, School of Health, Social Determinants of Health Research Center,  
Mashhad University of Medical Sciences, Mashhad, Iran, email: behnam\_barikbin@yahoo.com

<sup>c</sup>Department of Civil Engineering, Isra University, Amman, Jordan, email: ethar.al-essa@pg.canterbury.ac.nz

<sup>d</sup>Department of Environmental Health Engineering, School of Health, Birjand University of Medical Sciences,  
Birjand, Iran, email: khosravi.r89@gmail.com

<sup>e</sup>Building and Construction Techniques Engineering Department, Al-Mustaqbal University College, 51001 Hillah,  
Babylon, Iraq, email: tariq.jwad@mustaqbal-college.edu.iq

<sup>f</sup>Cellular and Molecular Research Center, Birjand University of Medical Sciences, Birjand, Iran,  
Tel. +9856-32432573; Fax: +9856-32432573; email: Negin.Nasseh2020@gmail.com

Received 25 April 2022; Accepted 17 October 2022

---

### ABSTRACT

In this study, we investigated the influence of a novel magnetic activated carbon (MAC) nanocomposite coated with CuS (MAC/CuS) on the successful removal of tetracycline (TC) molecules from aqueous solutions via adsorption. The physical and structural properties of the synthesized sorbent were determined using the field-emission scanning electron microscopy, Brunauer–Emmett–Teller, X-ray diffraction, Fourier-transform infrared spectroscopy, and vibrating-sample magnetometer techniques. Equilibrium isotherms and adsorption kinetics were studied. Additionally, the effects of pH (3, 5, 7, and 9), TC concentration (5–100 mg/L), MAC/CuS dosage (0.025–2.5 g), temperature (5°C, 10°C, 20°C, 40°C, and 50°C), and contact time (from inception to 200 min) were extensively examined. Our results revealed that the highest TC removal percentage was approximately 70% under optimal conditions (pH = 9, contact time = 200 min, nanocomposite dosage = 2 g/L, and temperature = 20°C). Modelling of the experimental data using isothermal models indicated that the TC adsorption process followed the Temkin model. Thermodynamic analyses revealed that the adsorption process was spontaneous and exothermic. A kinetic study demonstrated that the pseudo-second-order kinetic model was best for describing TC adsorption. This work presents a magnetic activated carbon nanocomposite coated with CuS as a high-efficiency adsorbent for the remediation of wastewater loaded with TC.

**Keywords:** Magnetic activated carbon; CuS; Nanocomposite; Adsorption; Tetracycline removal; Aqueous solution

---

\* Corresponding author.

## 1. Introduction

The presence of toxic and carcinogenic contaminants in aqueous media, including pharmaceutically activated compounds (PhACS), represents a possible threat to human health and to the safety of the surrounding environment [1,2]. Tetracycline (TC) is one of the main groups of antibiotics that are naturally obtained from semisynthetic processes or the fermentation of specific fungi, and it is commonly used in agriculture, aquaculture, veterinary drugs, and for the treatment of infectious diseases [3]. After human and animal consumption, this antibiotic is partially adsorbed by organisms and enters the sewage system through urination, defecation, or the release of surplus drugs, and it can ultimately lead to severe unknown or suspicious ecological and human health consequences [4,5]. Chronic residual doses of TC in water cause permanent discoloration of teeth in prenatal individuals and during childhood and adulthood. Exposure to this compound can also result in the production of microvascular adipose tissue in the liver and skin sensitivity to ultraviolet (UV) radiation. Additionally, tetracycline exerts destructive effects on microbial respiration, nitrification, and reduction of trivalent iron in the soil environment. Therefore, due to the high human consumption of antibiotics, the concentration of these drugs in water in the environment increases and cause water quality to become decreased [6]. Moreover, the removal of TC using typical water treatment and sewage technologies is an incomplete process [7], as pharmaceutical antibiotics (TC) possess a multipolar structure that increases the chemical stability of TC and thus allows for a relatively long half-life for this drug in the environment [8]. Therefore, there has been increasing interest in developing effective and economical technologies for TC filtration.

Currently, treatment technologies for remediating pharmaceutical pollution in water and wastewater mainly include advanced oxidation processes [9], ozonation [10], coagulation [11], biological methods [12], and adsorption [13]. One of the most effective methods for removing TC from water is adsorption due to its numerous advantages such as simple functionality, rapid removal, lack of secondary contamination, and low cost and energy consumption [4–14]. A high specific surface area and rich porous structure are considered as essential characteristics for an effective adsorbent. A high specific surface area can allow for sufficient adsorption [15]. Different substances have been used to adsorb TC from aqueous media, including smectite clay [16], montmorillonite [17], rectorite [18], palygorskite [19], chitosan microparticles [20], aluminum oxide [21], activated carbon [22], and single- and multi-walled carbon nanotubes [23]. Activated carbon is an effective sorbent due to its high adsorption capacity, low price, and porous structure, and activated carbon allows for enhancement of water quality by facilitating the elimination of pollutants from aqueous media [24]. However, problems such as dispersion, turbidity, and high revival costs have limited the large-scale application of the substances described above [25]. Therefore, the combination of activated carbon with magnetite nanoparticles ( $\text{Fe}_3\text{O}_4$ , MNPs) coated with CuS represents a promising approach to enhance the adsorption of contaminants based on the desirable properties of

magnetite nanoparticles (high specific surface area, high adsorption capacity, and superparamagnetic properties) that enable them to facilitate their optimal use and produce wastewater with a very low turbidity value [25,26]. Additionally, after the reaction with the target compound or contaminant is completed, magnetite nanoparticles can be easily separated and removed from the liquid media by applying a magnetic field [27]. Moreover, copper sulfide (CuS) with a 2 eV bandwidth is a key compound possessing superior properties, including physicochemical structure (e.g., high chemical stability at different pH levels and high surface area), electrical conductance, and magnetism properties [28]. Furthermore, it is relatively inexpensive, harmless, environmentally friendly, and exhibits a high oxidation ability [29].

Activated carbon is produced using various raw materials, including cellulosic raw materials (e.g., wood, coconut shells, fruit pyrenes, and other agricultural wastes) [30], raw carbon materials (e.g., coal, petroleum coke, and bitumen) [31], and raw polymers (e.g., rubber and plastic waste) [32]. More recently, agricultural by-products and plants (e.g., almonds) have been commonly used to produce activated carbons due to their availability in large quantities and their low production cost [33]. Almond is a local plant in the Southern Khorasan province in eastern Iran and is considered to be a commercial and economic product of the region. Almond green hull that is separated and released into the environment as waste after the fruit is picked from the tree can be used as a base for producing activated carbon [34]. Sono chemistry is the product of the chemical and physical effects of ultrasound waves on the chemical reactions. The conditions required for ultrasound radiation to obtain activated carbon are easier compared to conditions required for other activation methods that require an ultrasonic source and an aqueous medium [35]. Ultrasonic radiation in aqueous solvents forms and destroys gas bubbles (cavitation), thus resulting in a temporary rise in pressure and temperature that ultimately leads to the formation of OOH and OH free radicals. These radicals diffuse in water and oxidize minerals [36].

In this study, the raw biological material (almond green hulls) was initially magnetized and then subjected to carbonation and activation. Subsequently, magnetically activated carbon was prepared via a new method using ultrasonic waves. Finally, CuS was loaded onto the magnetically activated carbon to obtain the new nanocomposite MAC/CuS that was used for the adsorption of TC antibiotics.

## 2. Materials and methodology

### 2.1. Materials

The chemicals used in this study were copper sulfate ( $\text{CuSO}_4$ ), sodium thiosulfate ( $\text{Na}_2\text{S}_2\text{O}_3$ ), ethylene glycol ( $\text{C}_2\text{H}_6\text{O}_2$ ), trivalent iron chloride ( $\text{FeCl}_3 \cdot 6\text{H}_2\text{O}$ ), divalent iron chloride ( $\text{FeCl}_2 \cdot 4\text{H}_2\text{O}$ ), hydrochloric acid (HCl), caustic soda (NaOH), phosphoric acid ( $\text{H}_3\text{PO}_4$ ), and ethanol ( $\text{C}_2\text{H}_5\text{OH}$ ), and all of these chemicals were purchased from Merck Company (Germany) TC hydrochloride salt ( $\text{C}_{22}\text{H}_{24}\text{O}_8\text{N}_2 \cdot \text{HCl}$ ) was purchased from Sigma-Aldrich Company (America). A stock solution (1,000 mg/L) was prepared by dissolving

TC hydrochloride in deionized water. This solution was prepared as required and stored in a refrigerator at 4°C until it was supplied to batch bottles.

## 2.2. Preparation of almond green hulls

A specific quantity of almond green hull (AGH) was collected from Nutex Trading Company (Iran). To obtain nanoscale particles, almond green hulls were powdered and passed through a 60-mesh screen (250 μm) and then through a 200-mesh screen (75–250 μm). The collected powder was used to produce a MAC/CuS nanocomposite.

## 2.3. Synthesis of the MAC/CuS nanocomposite

The MAC/CuS nanocomposite was successfully synthesized according to a previously published procedure [37]. This synthesis was accomplished through the use of four steps (magnetization, carbonation, post-activation, and loading copper sulfide). Magnetization samples of the screened AGH powders were prepared in three stages. In the first stage, 200 mL of distilled water was deoxygenated by placing the distilled water onto the mixer in the presence of nitrogen gas for 30 min under heating conditions of 60°C–70°C. In the second-stage, 6 g of the screened powder was dissolved in sodium hydroxide (100 mL, 0.1 M) and shaken at 300 rpm for 30 min. In the third stage, 2 g of iron salt (FeCl<sub>3</sub>) and 1 g of iron salt (FeCl<sub>2</sub>) were added to the deoxygenated water. Subsequently, the resulting solution of screened powder and sodium hydroxide obtained from stage two was added to the resulting solution of iron oxides obtained from stage three under vigorous stirring at 400 rpm for 1 h. During this stage, the nitrogen sparging was ceased, and the temperature was maintained at 60°C. Finally, the generated magnetic almond green hulls (MAGH) were washed with distilled water several times until the pH level changed from alkaline to neutral. Next, the MAGH samples were dried in an oven at 80°C for 3 h. Finally, the MAGH sample was saturated with 10% phosphoric acid and maintained in an isolated medium for 48 h. It was then dried in a vacuum oven for 3 h at 75°C [37].

For the carbonization step, the synthesized MAGH samples were placed inside a cylindrical steel reactor to prevent oxygen diffusion and then transferred to a programmable HL40P controller for 2 h. During this time, the oven temperature was raised to 550°C at a rate of 300 degrees/h [35].

Subsequently, the activation step was performed, where ultrasonic waves were used as the activating agent. This was accomplished by submerging magnetic carbon powder in normal HCl<sub>3</sub> and dispersing it for 1 h using an Elmasonic E30H ultrasonic device at 37 kHz [38].

To upload the copper sulfide onto the activated magnetic carbon surface, 0.15 g of the prepared magnetic activated carbon was dispersed in 20 mL of ethylene glycol (EG) for 30 min using an ultrasonic device. These MAC were placed into a 500 cc volumetric flask inside an oil bath at 120°C. Then, 0.8 g of CuSO<sub>4</sub> was added to the suspension. After completing the dissolution of copper sulfide inside the volumetric flask, 1.9 g of Na<sub>2</sub>S<sub>2</sub>O<sub>3</sub> that was previously dissolved in 20 mL of EG was poured into the resulting MAC and CuS suspensions. Next, the reflux operation was performed at 140°C for 90 min. After cooling the volumetric

flask, the resulting MAC/CuS nanocomposite samples were separated using an N<sub>42</sub> magnet, washed once with ethanol, and washed again with deionized water. Finally, the MAC/CuS nanocomposite was dried in a vacuum oven at 80°C for 5 h [39].

## 2.4. Characterization of the MAC/CuS nanocomposite

To investigate the shape, morphology, and diameter of the synthesized MAC/CuS nanocomposite, a field-emission scanning electron microscopy (FESEM) analyzer was applied using a FESEM device (Sigma VP, ZEISS Co., Germany). The surface areas (S<sub>BET</sub>), approximate pore volume, size, and sample porosity values were calculated according to Brunauer–Emmett–Teller (BET) method using a BELSORP Mini Sorption Analyzer (Microtrac Bel Corp. Co., Japan). X-ray diffraction (XRD) analysis was employed to determine the structural properties of the MAC/CuS nanocomposite using an X'Pert PRO device (Panalytical Co., Netherlands). Fourier-transform infrared spectroscopy (FTIR) analysis was performed using a Spectrum Two (PerkinElmer Co., America) at the range of 400 to 4,000 cm<sup>-1</sup> wavelengths to identify the functional groups present in the obtained MAC/CuS nanocomposite. A vibrating-sample magnetometer (VSM) device (LBKFB, Meghnatis Daghigh Kavir Co., Iran) was used to estimate the magnetization of the MAC/CuS nanocomposite sample.

## 2.5. Batch experiments

The TC adsorption tests were conducted in a batch system using several glass flasks. To accomplish this, a specific amount of MAC/CuS was mixed with 400 mL of TC solution at different concentrations at 300 rpm. The effects of experimental variables such as pH (3, 5, 7, and 9), TC concentration (5–100 mg/L), MAC/CuS dosage (0.025–2.5 g/L), temperature (5°C, 10°C, 20°C, 40°C, and 50°C), and contact time (from inception to 200 min) were evaluated. The pH values of the solutions were adjusted using hydrochloric acid (HCl, 0.1 mM) and sodium hydroxide (NaOH, 0.1 mM) and measured using a HACH Hq411d pH meter (America).

Finally, the samples were acquired at different adsorption times and after magnetic separation of the MAC/CuS nanocomposite, and the remaining TC concentration was measured using a UV–visible T80p spectrophotometer at a wavelength of 358 nm [40]. Each experiment was performed in triplicate, and the average value was reported. The TC removal efficiency (*R* [%]) and adsorption capacity (*q<sub>e</sub>*) were calculated using Eqs. (1) and (2) as follows:

$$R(\%) = \left(1 + \frac{C_e}{C_0}\right) \times 100 \quad (1)$$

$$q_e = \frac{(C_0 - C_e) \times V}{M} \quad (2)$$

where *R* (%) is the percentage removal of TC, *C<sub>0</sub>* is the initial concentration of TC (mg/L), *C<sub>e</sub>* is the remaining concentration of TC (mg/L), *q<sub>e</sub>* is the equilibrium adsorption capacity (mg/g), *V* is the sample volume (L), and *M* is the mass of the adsorbent (g).

To determine the remaining concentration and adsorption at a specific adsorption time, the  $C_e$  and  $q_e$  values were denoted by  $C_t$  and  $q_t$ , respectively.

### 2.6. Determining of $pH_{zpc}$ of the adsorbent

The isoelectric point pH of MAC/CuS was evaluated by preparing six samples. Each sample contained 100 mL of NaCl (0.1 mM), and the initial pH values of these solutions were adjusted to 2, 4, 6, 8, 10, and 12. Then, 0.2 g of the MAC/CuS nanocomposite was added to each sample and shaken for 48 h. The final pH of the samples was measured. The intersection of the  $pH_{initial}$  and  $pH_{final}$  curves is referred to as the isoelectric point pH [41].

### 2.7. Models and statistical parameters

For the isotherm, kinetic, and thermodynamic studies, the results of the experiments of the MAC/CuS nanocomposite adsorption capacities at different pollutant concentration, adsorption time, and solution temperature were used, respectively. The equations of these studies and some background information are illustrated in sections: S1, S2, and S3 (Supporting information). In addition, the root mean square error (RMSE) was calculated [Eq. (3)] to evaluate the isotherm and kinetic models. The smaller the RMSE values, the more accurate the fitness of the model becomes [42–47].

$$RMSE = \sqrt{\frac{1}{P-2} \sum_{i=1}^P (q_e - q_c)^2} \quad (3)$$

where  $q_c$  is the model fitness value,  $q_e$  is the value obtained from the test, and  $P$  is the number of test parameters.

## 3. Results and discussion

### 3.1. Characterizations

#### 3.1.1. FESEM analysis

The FESEM micrographs are presented in Fig. 1. Almond-green hulls were observed in the pores (Fig. 1a). Moreover, a micrograph of the magnetic almond green hull (Fig. 1b) clearly indicates the uniform presence of iron particles on the green hull. Additionally, a carbonated magnetic almond green hull (Fig. 1c) possessing few pores on the progenitor carbon surface was detected. Similar results were observed in a previous study [48]. Fig. 1d presents the magnetic activated carbon of the almond green hull with numerous regular pores on the surface. This can be explained by the addition of hydrochloric acid to the magnetic green hull and its placement in the ultrasound waves that created these pores. This was confirmed by a previous study [49] that reported that in aqueous media, ultrasonic waves create

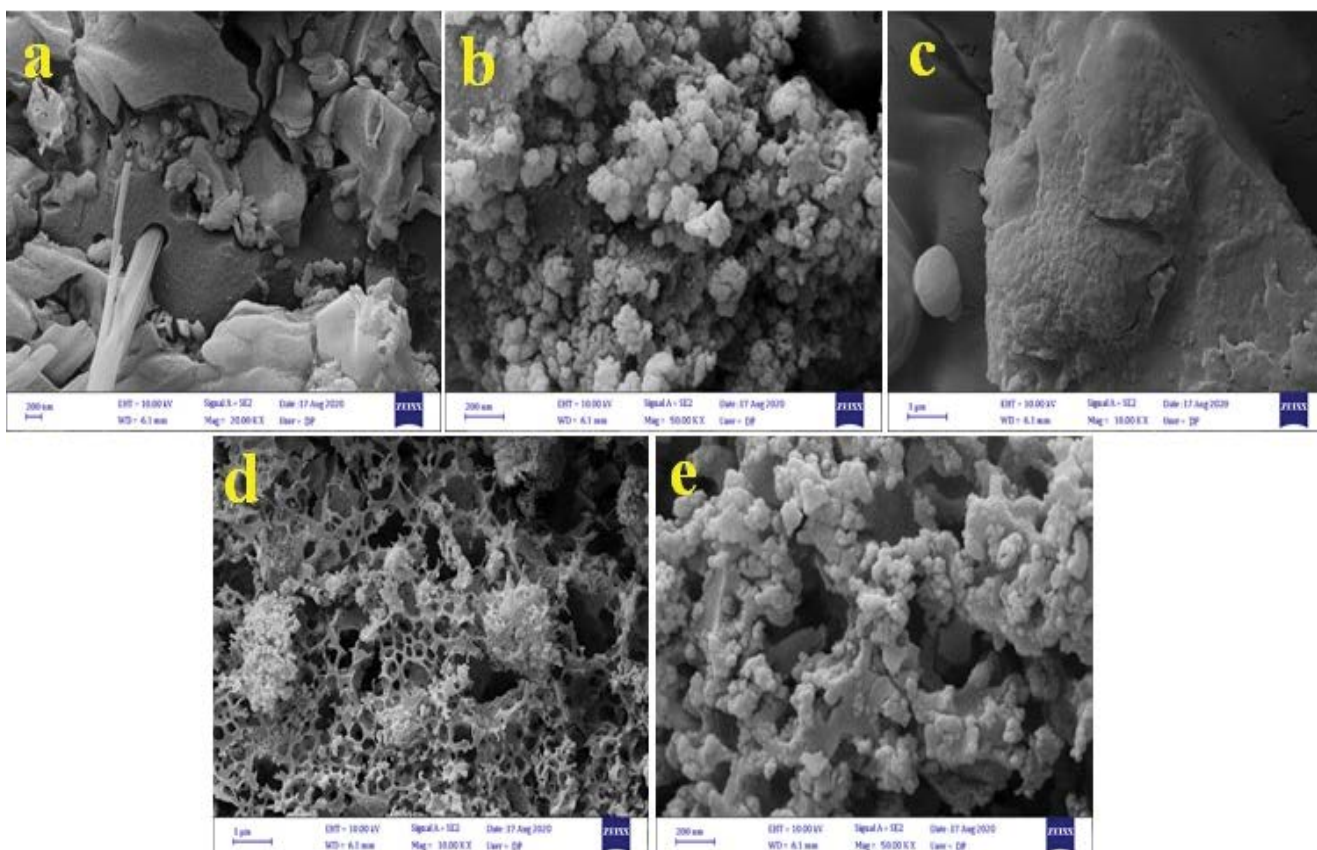


Fig. 1. FESEM images of almond green hull (a,b), carbonated almond green hull (c), magnetized almond green hull (d), and the MAC/CuS nanocomposite (e).

cavitation and produce free radicals, and this is followed by the oxidation of mineral compounds. Fig. 1e presents the final composite after loading copper sulfide onto the activated carbon (magnetic AC/CuS) resulting from the magnetic almond green hull, and the results suggest that copper sulfide settled properly onto the activated carbon.

### 3.1.2. Surface area (BET) analysis

The results of the surface area (BET) analysis revealed that the activation process utilizing ultrasonic waves effectively improved the special surface of the carbon. Additionally, the specific surface area of the almond green hull powder was 13.032 m<sup>2</sup>/g, thus suggesting a relatively low surface-to-volume ratio. There were few pores on the almond green hull raw powder surface that was smooth and relatively level as indicated in the FESEM images (Fig. 1a). Continuing the synthesis of the composite reduced the specific surface area of the magnetic raw powder to 8.44 m<sup>2</sup>/g via carbonation. It is assumed that under oxygen-free conditions in the oven, the burning of certain compounds would form bitumen-like substances on the sorbent surface. This reduces the specific surface area by plugging the pores [1]. After activation of the carbonated substance, the specific surface area significantly increased and reached 186.83 m<sup>2</sup>/g. This indicated that during the activation process, the bitumen-like substances were properly separated from the surface, and the sorbent pores were eliminated. These results were in agreement with the FESEM results. Furthermore, according to the BET analysis results, loading copper oxide onto the magnetized composite significantly reduced the surface-to-volume ratio of the composite to 14.79 m<sup>2</sup>/g, and this implied that copper sulfide was placed properly on the sorbent surface and its pores. This observation is in good agreement with those reported in a previous study [50]. Additionally, the average pore diameter analysis results were 3.75, 20.32, 7.92, and 39 nm for the almond green hull, magnetic carbon, magnetic activated carbon, and magnetic activated carbon coated with CuS, respectively. This may be explained by the possibility that carbonating almond hulls under anaerobic conditions created numerous pores on the surface of the biosorbent. However, bitumen-like substances filled these pores and increased the average particle diameter of the carbon AGH. In contrast, during the activated carbon process ultrasonic waves and diluted hydrochloric acid solution removed the bitumen-like substances from the sorbent surface and increased the number of pores on the carbon surface. Accordingly, the average particle diameter was decreased to 7.92 nm. Additionally, loading copper sulfide onto activated magnetic carbon significantly increased the mean particle diameter to 39 nm. The results of the BET analysis revealed that AC/CuS is a good treatment agent and suitable material to be used in adsorption process.

### 3.1.3. XRD analysis

X-ray diffraction analysis was performed to identify the crystalline structure of Fe<sub>3</sub>O<sub>4</sub> in the porous activated carbon. The XRD patterns of the magnetic AC and the magnetic

AC/CuS nanocomposite at 2θ are presented in authors' previous article 37. The peak values were obtained corresponding to the presence of iron in the activated carbon, and crystal plates were observed corresponding to the reverse spleen cube of Fe<sub>3</sub>O<sub>4</sub>. The results of the magnetic AC analysis revealed that the peaks were 30.78, 35.46, 53.84, 57.52, 63.02, and 74.53 (ICSD # 159976). Similar observations were reported by Depci et al. and Anyika et al. [51,52]. Additionally, the corresponding magnetic AC/CuS peaks were 29.35, 31.85, 32.13, 48.04, 51.09, and 59.89 (ICSD # 158743). Furthermore, the average crystallite size that was calculated from the XRD results using the Scherrer equation [Eq. (4)] [53] indicated that the full-width-at-half-maximum wavelength was 29 nm at the most severe diffraction peak. This is comparable to the crystalline size of commercial magnetite (28 nm) that is described by the following equation [54]:

$$D = \frac{0.98\lambda}{\beta \cos\theta} \quad (4)$$

where  $D$  is the particle diameter,  $\beta$  is the peak width at half-maximum height,  $\theta$  is the diffraction angle at the peak stage, and  $\lambda$  is the X-ray wavelength ( $\lambda = 0.1540$  nm).

Additionally, it has been reported that activated carbon did not alter the crystalline size of magnetite [55]. These results reveal that activated carbon does not influence the crystalline size domain of the magnetite particles, and this suggests that magnetic activated carbon at 29 nm is effective and useful for adsorption. However, as FESEM analysis indicated that nanoparticles tend to accumulate due to their magnetic properties, the particle size based on FESEM images (64 nm) was higher than the value obtained from the Scherrer equation (29 nm). The reason for the difference could be that XRD analysis often indicates the crystal size, whereas FESEM analysis reveals the particle size, and as presented, one particle consists of multiple crystals and can thus explain this large scale. In fact, the results of XRD analysis confirms that magnetic AC/CuS nanocomposite was successfully prepared in this study.

### 3.1.4. FTIR analysis

FTIR was performed to characterize the sorbent and sorbent-sorbate interactions in five samples that included the almond green hull, magnetic AGH, magnetic carbon, magnetic AC, and magnetic AC/CuS. The FTIR spectra for each sample are illustrated in authors' previous article 37. As presented in the results for all five samples, the broad peaks are in the range of 1,000 to 1,200 cm<sup>-1</sup>. These results indicate the presence of a C–O bond [51–56]. Additionally, the FTIR spectra of all five samples indicated that the peaks that are centered at 1,443; 1,608; 2,923 and 3,421 cm<sup>-1</sup> are related to the presence of N–O, C=O, C–H, and O–H functional groups, respectively [25]. Moreover, the spectrum of AGH exhibited a small peak at 1,741 cm<sup>-1</sup>, thus signifying the presence of N–H functional group [57].

Furthermore, the FTIR figure presents a clear intense peak from 500 to 1,000 cm<sup>-1</sup> in magnetic AGH, magnetic carbon, and magnetic activated carbon, respectively. This may be attributed to the presence of the Fe–O–OH and

Fe–O agent groups. This indication was based on previously reported peaks in this region [51–56]. Anyika et al. [51] reported that the FTIR spectrum of magnetite appears at  $552\text{ cm}^{-1}$ . These results confirm the presence of magnetite particles on the surface. Additionally, the FTIR figure indicates that the carbonation of magnetic AGH eliminated the peak specific for the C–O functional group ( $562\text{ cm}^{-1}$  wavelength). This occurs due to carbon burning that takes place during the carbonation process in the high-temperature oven, and the peak corresponding to iron thus becomes more clearly visible [37]. Additionally, the spectra of magnetic carbon and magnetic activated carbon exhibit broad peaks at  $2,300\text{ cm}^{-1}$  that correspond to O–H and P–O (phosphate) functional groups. This is based on the use of phosphoric acid for carbonating magnetic AGH [58]. CuS-coated magnetic AC analysis also revealed that the adsorption band at  $2,317\text{ cm}^{-1}$  corresponds to the Fe–Cu bond vibrations and overlaps the O–H and P–O functional groups [59]. Finally, the adsorption band at the  $480.17\text{ cm}^{-1}$  spectrum corresponds to metal bond vibrations with sulfur heteroatoms, and the most probable bond is CuS [60]. The FTIR groups indicated on the AC/CuS surface give an indication that this adsorbent has high ability to adsorb different pollutants from aqueous solution.

### 3.1.5. VSM analysis

Vibrating-sample magnetometer (VSM) analysis was performed as presented in the authors' previous article 37 to analyze the biosorbent in each of the synthesis stages (magnetization, carbonation, post-activation, and loading copper sulfide). According this reported the magnetic properties of magnetic AGH, magnetic carbon, magnetic AC and magnetic AC/CuS are 0.5, 5.1, 16.8 and 9.2 emu/g, respectively. According to the results of the VSM analysis, AGH possessed no magnetic properties despite the presence of iron in its composition. This may be due to the presence of various compounds such as carbon in AGH. However, almond green hulls acquire their magnetic properties due to the removal of these compounds during composition in a high-temperature oven ( $550^\circ\text{C}$ ) [35]. Meanwhile, the formation of bitumen-like substances resulting from the burning of a number of minerals on the adsorbent surface under anaerobic oven conditions degrades the magnetic properties of carbon. However, these bitumen-like substances are removed from the adsorbent during the activation process, and this increases their magnetic properties. Moreover, the results revealed that the activated carbon obtained from magnetic AGH exhibited the best magnetic properties. Finally, although placing copper sulfide on the activated carbon reduced the magnetic properties, this compound could be quickly separated from the solution using an external magnetic field.

## 3.2. Factors affecting TC adsorption efficiency

### 3.2.1. Effect of pH value

The effect of pH level in regard to sufficient TC ( $20\text{ mg/L}$ ) adsorption onto MAC/CuS nanocomposite ( $0.25\text{ g/L}$ ) (Fig. 2a) indicated a strong interrelationship

between TC adsorption and pH value. It was clearly noted that the adsorption efficiency was 5.94% at a pH value of 3, and this efficiency increased as the pH value was increased and reached a maximum adsorption of 34.69% at a pH value of 9. It is generally recognized that the pH level determines the behavior of both adsorbents and contaminants. Specifically, the pH value determines the TC ionic type and the adsorbent surface charge. Consequently, this would affect the adsorption process of the adsorbate and also the functional groups between the adsorbent surface and the  $\pi$ – $\pi$  reaction mechanism and cation– $\pi$  (cationic bond) banding [61–63]. TC is an amphoteric molecule that possesses multiple ionizing functional groups. In aqueous media, this antibiotic exhibits various pKa levels at pH values of 3.3, 7.7, and 9.7. Specifically, at pH values of less than 3, TC appears in a protonated form ( $\text{H}_4\text{TC}^+$ ), at a pH range of  $3 < \text{pH} < 8$ , TC is neutral ( $\text{H}_3\text{TC}^0$ ), and at a range of  $8 < \text{pH} < 10$ , TC appears in a monoanionic form ( $\text{H}_2\text{TC}^-$ ) (Fig. 2b) [64]. Therefore, the effect of pH on the TC adsorption removal rate can be attributed to the dominance of one or multiple types of antibiotics at various pH levels. The TC adsorption rate changes that occur in acidic solutions ( $\text{pH} < 3$ ) are due to the electrostatic repulsion force between cationic TC molecules and the positive charge of the nanoparticle surfaces [65]. When the pH is increased (to 8), the TC molecules become neutral, and as a result, the contaminant adsorption by the MAC/CuS nanosorbent becomes negligible. Furthermore, a likely reason for TC molecule adsorption on the nanosorbent at pH values of greater than 8 could be  $\pi$ – $\pi$  electron donor-acceptor reactions that occur between TC and sorbent molecules [66]. The MAC/CuS surface charge was calculated separately using the  $\text{pH}_{\text{zpc}}$  test (Fig. 2c). The results obtained from the adsorbent surface charge analysis suggested that the adsorbent possessed a neutral  $\text{pH}_{\text{zpc}}$  ( $\text{pH}_{\text{zpc}} = 7$ ). It is well known that the adsorbent surface charge is positive at pH levels that are below  $\text{pH}_{\text{zpc}}$  and negative at pH levels that are below  $\text{pH}_{\text{zpc}}$ . Thus, at pH levels that are lower than  $\text{pH}_{\text{zpc}}$ , TC adsorption is dependent upon the electrostatic reaction between the positive surface of the sorbent and the negatively charged TC molecules. In the pH range of 6–7, the adsorption process is physical due to the negative sorbent surface charge and the TC molecules. Under basic conditions, the dominant TC adsorption mechanism is the electrostatic reaction between amine proton groups (on the 4 ring [ $\text{C}_4$ ] and with a  $\text{pK}_a$  of 7.9) and the negative adsorbent surface [61–67].

In the present study, the highest TC adsorption removal rate was obtained at an alkaline pH ( $\text{pH} = 9$ ). This result is in agreement with the results obtained by Zhao et al. [68] who reported that the optimal pH for TC adsorption on goethite is 8.

### 3.2.2. Effect of MAC/CuS nanocomposite dosage

The amount of adsorbent is an important parameter that influences the adsorption removal rate and capacity. The relationship between TC adsorption efficiency and the adsorbent dosage (Fig. 3) revealed that increasing the adsorbent concentration from  $0.025$  to  $1.5\text{ g/L}$  resulted in a rapid increase in the adsorption removal rate from 20.92%

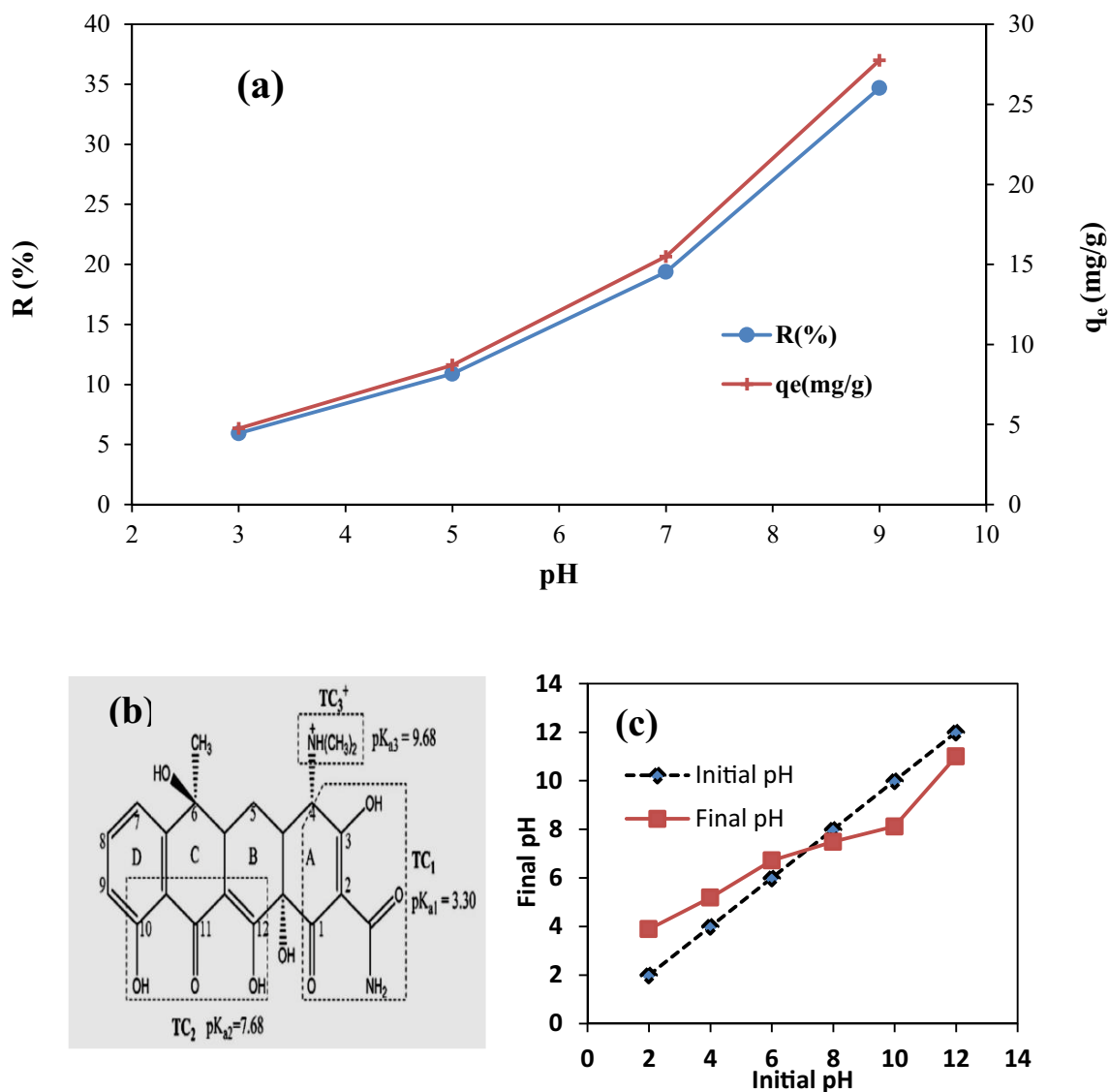


Fig. 2. (a) Effect of pH value on the adsorbent efficiency (TC concentration: 20 mg/L; adsorbent dosage: 0.25 g/L; contact time: 60 min; ambient temperature). (b) Structure of tetracycline. (c) Determining the  $pH_{zpc}$  value of the MAC/CuS nanocomposite.

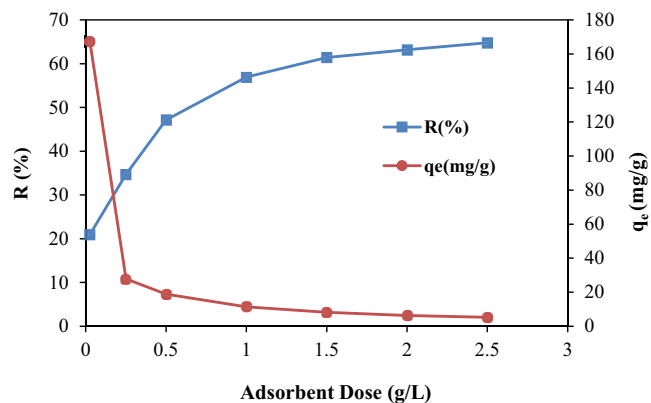


Fig. 3. Effect of MAC/CuS dosage on the adsorption efficiency (TC concentration: 20 mg/L; contact time: 60 min; pH = 9; ambient temperature).

to 61.43% while the adsorption capacity was decreased from 167.36 to 8.19 mg/g. However, increasing the adsorbent amount from 1.5 to 2 g/L resulted in a slower increase in adsorption removal rate (from 61.43% to 63.16%) and reduction in adsorption capacity (from 8.19 to 6.316 mg/g). After increasing the amount of adsorbent from 2 to 2.5 g/L no change was observed in regard to the TC adsorption efficiency and capacity. Therefore, the sorbent dosage of 2 g/L was determined to be optimal for TC adsorption. The increase in TC removal efficiency with increasing adsorbent dosage may be due to increased adsorbent dosage causing an increase in the active sites and contact surface of the adsorbent. Additionally, even if the amount of nanosorbent is increased due to a certain amount of TC being adsorbed on the sorbent, the concentration of TC in the reaction medium and, subsequently, the contact of TC with the nanosorbent will decrease significantly. As a result, the

TC removal efficiency was slightly improved. However, due to the constant concentration and volume of the TC solution, increasing the adsorbent dose causes the active sites of the adsorbent to remain unsaturated, and with an increase in the adsorbent dose, the accumulation of the adsorbent occurs in the aqueous solution and the actual adsorption capacity of the adsorbent decreases. Finally, the tetracycline removal efficiency was also decreased [69,70].

### 3.2.3. Effect of TC concentration and contact time

To determine the effect of the initial TC concentration and contact time on the adsorption efficiency, various concentrations of TC (5, 10, 20, 50, and 100 mg/L) were exposed to the optimal dosage of MAC/CuS nanocomposite (2 g/L) at optimal pH (9), and Fig. 4 presents the results. The results indicated that over time, the adsorption efficiency increased and the adsorption intensity decreased. The adsorption efficiency increased from 5 to 60 min. For example, in 20 mg/L of TC, the adsorption ratio from 5 to 60 min increased from 29.92% to 63.16%. However, the removal rate was relatively low from 60 to 200 min, and after this, the adsorption amount remained constant. Specifically, equilibrium between the solid phase and the solution was reached after 60 min. Therefore, the adsorption equilibrium time was established as 60 min. According to the results presented in Fig. 4, increasing the initial TC concentration reduced the nanosorbent removal efficiency due to the limited adsorption area in the sorbents that were more rapidly saturated after increasing the initial contaminant concentration and reducing the removal efficiency. Another reason for this phenomenon could be the selective adsorption of a specific contaminant by the sorbent. In these cases, there are specific places on the sorbent for the adsorption of specific contaminants that are only involved in the adsorption process. Therefore, increasing the contaminant concentration reduces adsorption due to the fixed positions of adsorption. These results are consistent with the results of the studies of Zhang et al., Zhu et al., and Ahmad et al. [5,71,72].

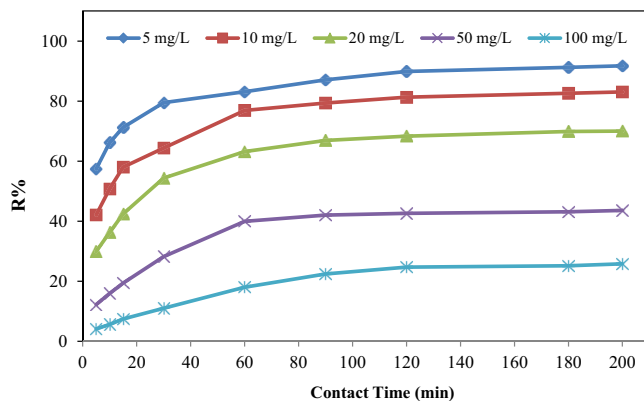


Fig. 4. Effect of TC concentration on the adsorption process facilitated by MAC/CuS (adsorbent dosage: 2 g/L; pH value at 9; ambient temperature).

### 3.2.4. Effect of temperature on TC adsorption

Fig. 5 presents the effect of the temperature on TC adsorption. Increasing the temperature significantly increased the removal percentage. Therefore, the increase in the removal percentage can be explained by the increase in the adsorption rate due to the endothermic process [73]. In the meantime, the adsorption of TC by the adsorbent used in this study mutates significantly up to 20°C, and no significant change occurs at temperatures of up to 50°C. Therefore, to save costs and energy, ambient temperature is considered to be optimal for the reaction conditions.

The solution temperature is a critical parameter that influences the adsorption process, as it may affect the suitability of the adsorbent [74]. The effects of temperature (5°C, 10°C, 20°C, 40°C, and 50°C) on the TC adsorption process were also studied. Fig. 5 clearly indicates that the adsorption removal rate was significantly increased (24%, 32%, and 68%) as the temperature was increased (5°C, 10°C, and 20°C). As the adsorption process is endothermic, the increase in the adsorption removal percentage can be attributed to the increase in the adsorption reaction rate due to the endothermic process. However, the removal rate of adsorption was not significantly altered between 20°C and 50°C. Therefore, these results suggest that the most suitable temperature is 20°C. Therefore, to save cost and energy, the ambient temperature was chosen as the optimal temperature for the reaction [73].

### 3.3. Isotherm model of TC adsorption onto the MAC/CuS nanocomposite

It is necessary in the adsorption treatment system to study the isotherms of equilibrium data to understand the adsorption mechanism. To achieve this goal, the isothermal data should be carefully modelled with the relevant isotherm models. In fact, the isotherm is the most important parameter in designing adsorbent systems and describing the relationship between the adsorbate concentration and adsorption capacity of the sorbent. In this study, Langmuir, Freundlich, and Temkin models were selected to study the effect of the equilibrium concentrations on the TC adsorption process. The fitting isotherm curves and parameters are

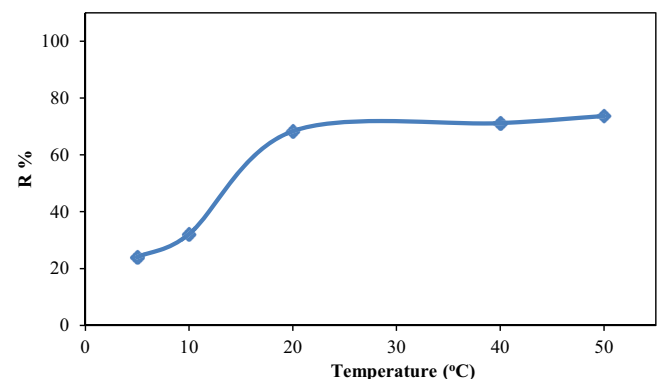


Fig. 5. Effect of temperature on TC adsorption using the magnetic MAC/CuS (adsorbent dosage of 2 g/L; pH value of 9; TC concentration of 20 mg/L; contact time of 120 min).

presented in Fig. 6 and Table 1, respectively. The Langmuir isotherm is the most common model based on the homogeneous (single-layer and uniform) adsorption of the adsorbate with the same energy across the adsorbent surface. In contrast, the Freundlich isotherm model is based on the heterogeneous (multi-layered) adsorption of the adsorbate on the adsorbent surface [75,76]. The Temkin isotherm considers the adsorbent–adsorbate interactions. In this model, extremely low and high concentrations of the adsorbate were neglected. Fig. 6 presents a non-linear model of isotherm data. These results suggest that the laboratory data were most consistent with the Temkin model output. Additionally, the results demonstrated that the coefficient of determination ( $R^2$ ) was 0.99 for both the Langmuir and Temkin isotherm models and 0.98 for the Freundlich isotherm model. From this perspective, the results indicated that Langmuir and Temkin adsorption isotherm models displayed the best fit for the adsorption. The RMSE parameter was smaller for the Temkin isotherm model (0.384) than it was for the Langmuir (0.780) and Freundlich (0.805) isotherm models. This indicates that the laboratory results were more consistent with the output of the Temkin isotherm

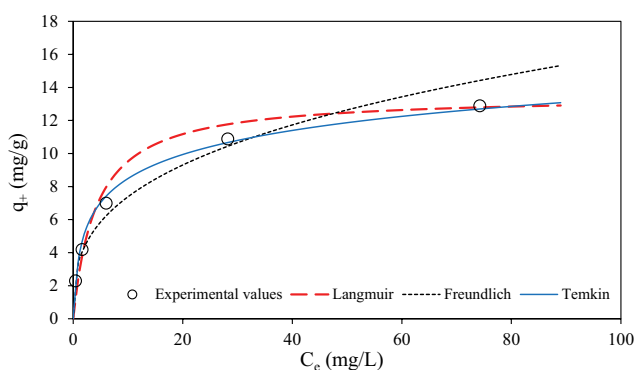


Fig. 6. Adsorption isotherms of TC onto MAC/CuS as fitted by the Langmuir, Freundlich, and Temkin models (pH value of 9; adsorbent dosage of 2 g/L; ambient temperature).

Table 1  
Isotherm parameters of TC adsorption onto the MAC/CuS adsorbent

Model	Value	Value
Langmuir	$R^2$	0.996
	$q_m$ (mg/g)	13.514
	$K_L$ (L/mg)	0.239
	RMSE	0.780
	$R^2$	0.980
Freundlich	$K_f$ (mg/g)	3.421
	$n$	2.994
	RMSE	0.805
	$R^2$	0.99
Temkin	$K_t$ (L/g)	5.69
	$B_t$ (J/mol)	1180
	RMSE	0.384

model. These results suggest that the Temkin model is an accurate adsorption isotherm model.

Furthermore, according to the information in Table 1, the Temkin constant ( $B_t$ ) that is defined as the energy adsorption variable was 1,180 [76], thus indicating that the adsorption reaction is endothermic at  $B_t$  values of greater than 1 and is exothermic at  $B_t$  values that are smaller than 1. These results suggest that in the range of concentrations tested in this study, the TC adsorption reaction that occurs on MAC/CuS is endothermic. This also implies an electrostatic interaction between the adsorbent and the adsorbate. Additionally, the heterogeneous pores on the MAC/CuS surface play a major role in the surface adsorption of TC [77]. In the analysis of Freundlich isotherm model, for optimal adsorption, the value of  $1/n$  should be less than one; in this study, it was 0.334, which indicates the optimal adsorption of TC molecules on the MAC/CuS nanocomposite [79–81].

Moreover, the estimated  $q_m$  of the Langmuir isotherm model was 13.5 mg/g, and this is very close to the  $q_m$  obtained from laboratory tests. Additionally, the dimensionless  $K_L$  parameter was between 0 and 1, and the  $n$  parameter in the Freundlich isotherm was 2.99.

The potential use of adsorbents on practical applications depends on the adsorbent capacity compared to other adsorbents used for target pollutant removal. Table 2 lists the values of the maximum adsorption capacity of MAC/CuS and several other adsorptive agents used for the removal of TC. It should be noted that MAC/CuS exhibited a higher adsorption performance for TC removal than did the other adsorbents. These results indicate that MAC/CuS is an optimal adsorbent. Furthermore, the MAC/CuS adsorption capacity was higher than was that of the uncoated MAC (Table 2), thus indicating the role of CuS nanoparticles in the improvement of MAC adsorption capacity for TC molecules. This is due to the enhancement of the absorptive properties of the MAC used after its modification with CuS particles as deduced in the properties study. In addition to its excellent efficiency, MAC/CuS can be separated from treated solution by an external magnetic field due to its great magnetic properties. As a result, this study suggests that the MAC/CuS nanocomposite as a suitable and favored adsorbent for TC wastewater treatment.

### 3.4. Kinetic analysis of TC adsorption onto the MAC/CuS adsorbent

Adsorption kinetics provides important information regarding the adsorption mechanism, adsorption removal rate, and time control during the adsorption process [83]. The pseudo-first-order kinetic model assumes that the removal rate of the adsorbate over time is directly correlated with changes in the saturated concentration and percentage of adsorbate removal achieved with time. The pseudo-second-order model assumes that two reactions (in parallel or series) affect adsorbate adsorption as follows: the first reaction rapidly and quickly reaches equilibrium, while the second is slow and continues for a longer time [84]. In the present study, the application of pseudo-first-order and pseudo-second-order kinetic models was evaluated through a kinetic study of the initial concentration of the adsorbent. Fig. 7 presents the kinetic analysis of

Table 2

Comparison of the maximum TC adsorption capacity ( $q_m$ ) of the used adsorbent and other adsorbents that were widely used in previous studies

Adsorbent	pH	TC initial concentration (mg/L)	Adsorbent dose (g/L)	Temperature (°C)	Adsorption time (min)	$q_m$ (mg/g)	References
<i>Streptomyces fradiae</i> biomass	6	100	2	–	240	38.61	[78]
CoFe <sub>2</sub> O <sub>4</sub> @methylcellulose	9	16	0.18	50	75	12.90	[79]
Biochars derived from waste fiberboard biomass	7	2.5–60	2.5	25	2,880	6.37	[80]
Nanocrystalline cellulose	5	1–25	1.5	25	120	7.73	[81]
Anaerobic granular sludge	4	80	–	35 ± 1	800	4.61	[82]
MAC	9	20	2	20	200	7.072	This study
MAC/CuS	9	20	2	20	200	13.514	This study

pH = 9; contact time = 200 min; nanocomposite dosage = 2 g/L; temperature = 20°C.

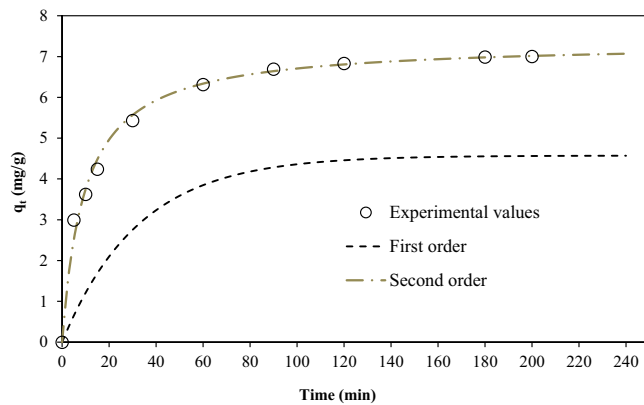


Fig. 7. Analysis of kinetic models of TC adsorption onto the MAC/CuS adsorbent (pH value of 9; adsorbent dosage of 2 g/L; ambient temperature).

TC adsorption by the MAC/CuS sorbent, and Table 3 provides the corresponding parameters and correlation coefficients. Comparing the  $R^2$  coefficient values of the three synthetic models, the adsorption was consistent with the pseudo-second-order model. From a reaction rate standpoint, the most important kinetics was the second order, and most adsorption processes with efficient adsorbents followed these kinetics. These results are consistent with those of Gao et al. [63] who reported that adsorption and removal of TC antibiotics by graphene oxide from aqueous solution demonstrated that the adsorption kinetics of this process were consistent with the pseudo-second-order kinetics model. Similarly, Yang et al. [70] reported that the adsorption kinetics with cobalt oxide nanoparticles coated with carbon followed pseudo-second-order kinetics. Based on these results, the pseudo-second-order model is the best model for use in this study. The explanation for this suggestion is that when adsorption occurs due to diffusion into a layer or boundary, most of the kinetics follow the first order. Meanwhile, second-order kinetics reveal that chemical adsorption is the stage that slows down the process and controls the adsorption processes [85,86].

Table 3

Kinetic parameters for TC adsorption onto the MAC/CuS adsorbent

Kinetic	Parameters	Results
First-order	$q_e$ (mg/g)	4.57
	$k_1$ (L/mg)	0.0307
	$h_0$	0.14
	$R^2$	0.99
	RMSE	2.46
Second-order	$q_e$ (mg/g)	7.35
	$k_2$ (L/mg)	0.01412
	$h_0$	0.76
	$R^2$	1.00
	RMSE	0.19

The results of the kinetic study agree with the findings of previous studies using adsorption and photocatalysis processes [88,89].

### 3.5. Thermodynamic analysis of the TC adsorption process

Fig. 8 presents the temperature and thermodynamics of TC adsorption by the magnetic nanocomposite. The thermodynamic parameters for the adsorption of TC on the synthesized nanocomposite are listed in Table 4. The negative symbol for the Gibbs free energy changes ( $\Delta G^\circ$ ) at all temperatures indicates the spontaneity of the adsorption process [87]. The positive  $\Delta H^\circ$  value suggests that the adsorption process was naturally endothermic. Therefore, increasing the temperature stimulates the adsorption capacity. A positive  $\Delta S^\circ$  value indicates the inclination of adsorption to the sorbent in the solution and certain structural changes in the adsorbent and adsorbate, thus revealing that the adsorption is irreversible and stable [74–82]. Additionally, a positive entropy change ( $\Delta S^\circ$ ) indicates that the degree of freedom (viscosity) of the intermediate solid–liquid state increases during adsorption [53].

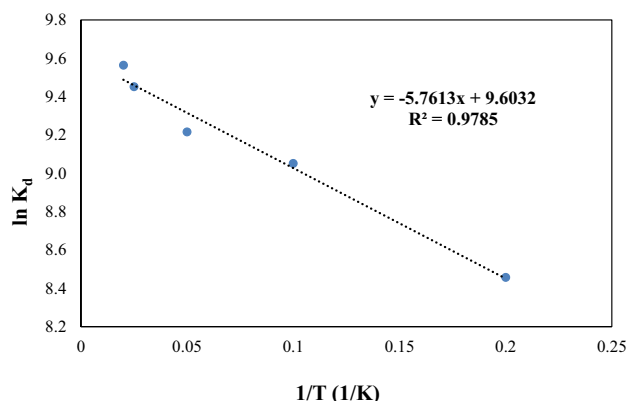


Fig. 8. Linear  $\ln k_d$  vs.  $1/T$  for adsorption of TC by the synthesized magnetic nanocomposite.

Table 4  
Thermodynamic parameters of TC adsorption by the synthesized nanocomposite

T (K)	$\Delta G^\circ$ (kJ/mol)	$\Delta H^\circ$ (kJ/mol)	$\Delta S^\circ$ (J/mol·K)
278	-20.876		
283	-22.222		
293	-24.426	0.0715	88.425
313	-26.315		
323	-27.223		

#### 4. Conclusion

This study was conducted to synthesize and evaluate the efficiency of a novel activated magnetic carbon nanocomposite coated with CuS in regard to removing TC from aqueous solutions. The results suggest that increasing the pH and adsorbent dosage while also reducing the initial pollutant concentration resulted in a reduced adsorption removal rate. The adsorption efficiency under the optimal adsorption conditions (pH value of 9, contact time of 200 min, MAC/CuS nanocomposite dosage of 2 g/L, temperature of 20°C, and tetracycline concentration of 20 mg/L) was approximately 70%. The data obtained from the Langmuir, Freundlich, and Temkin isotherms revealed that the TC adsorption process of the synthesized magnetic nanocomposite was compatible with the Temkin model. Thermodynamic studies indicated entropy changes ( $\Delta S^\circ$ ) of 88.43 J/mol·K, an enthalpy change ( $\Delta H^\circ$ ) of 0.072 kJ/mol, and negative Gibbs free energy ( $\Delta G^\circ$ ), thus suggesting that the adsorption process was spontaneous and endothermic. This nanocomposite was easily separated from the test environment through the use of an external magnetic field due to its excellent magnetic properties. Based on these results, the magnetic activated carbon nanocomposite obtained from almond green hull and coated with CuS can be recommended as an effective, low-cost, and promising adsorbent for the removal of TC antibiotics from aqueous solutions.

#### Acknowledgment

The authors sincerely thank Birjand University of Medical Sciences for financially supporting this study. The Ethics Committee of Birjand University of Medical Sciences (Iran) approved the study with the ethical and project code of IR.BUMS.REC.1399.036.

The authors would like to extend their gratitude to the Research and Innovation Department (Iran) and Al-Mustaqbal University College (Iraq).

#### References

- [1] M. Khodadadi, M.H. Ehrampoush, M.T. Ghaneian, A. Allahresani, A.H. Mahvi, Synthesis and characterizations of  $\text{FeNi}_3@\text{SiO}_2/\text{TiO}_2$  nanocomposite and its application in photocatalytic degradation of tetracycline in simulated wastewater, *J. Mol. Liq.*, 255 (2018) 224–232.
- [2] A. Tiwari, A. Shukla, D. Tiwari, S.M. Lee, Nanocomposite thin films  $\text{Ag}^0(\text{NP})/\text{TiO}_2$  in the efficient removal of micro-pollutants from aqueous solutions: a case study of tetracycline and sulfamethoxazole removal, *J. Environ. Manage.*, 220 (2018) 96–108.
- [3] H.U. Rasheed, X. Lv, W. Wei, D.K. Sam, N. Ullah, J. Xie, W. Zhu, Highly efficient photocatalytic degradation of the tetracycline hydrochloride on the  $\alpha\text{-Fe}_2\text{O}_3/\text{CN}$  composite under the visible light, *J. Environ. Chem. Eng.*, 7 (2019) 103322, doi: 10.1016/j.jece.2019.103322.
- [4] W. Xiong, G. Zeng, Z. Yang, Y. Zhou, C. Zhang, M. Cheng, Y. Liu, L. Hu, J. Wan, C. Zhou, Adsorption of tetracycline antibiotics from aqueous solutions on nanocomposite multi-walled carbon nanotube functionalized MIL-53 (Fe) as new adsorbent, *Sci. Total Environ.*, 627 (2018) 235–244.
- [5] H. Zhang, M. Shi, M. Xia, F. Zhao, The adsorption mechanism of montmorillonite for different tetracycline species at different pH conditions: the novel visual analysis of intermolecular interactions, *Water Air Soil Pollut.*, 232 (2021) 1–15.
- [6] L. Xu, J. Dai, J. Pan, X. Li, P. Huo, Y. Yan, X. Zou, R. Zhang, Performance of rattle-type magnetic mesoporous silica spheres in the adsorption of single and binary antibiotics, *Chem. Eng. J.*, 174 (2011) 221–230.
- [7] B. Debnath, M. Majumdar, M. Bhowmik, K.L. Bhowmik, A. Debnath, D.N. Roy, The effective adsorption of tetracycline onto zirconia nanoparticles synthesized by novel microbial green technology, *J. Environ. Manage.*, 261 (2020) 110235, doi: 10.1016/j.jenvman.2020.110235.
- [8] X. Bai, Y.J. Wang, Y. Li, X.J. Wang, Adsorption–photocatalytic remediation for series of tetracycline contaminants with  $\text{BiOCl}-\text{CdS}$  composite under simulated sunlight, *J. Taiwan Inst. Chem. Eng.*, 104 (2019) 94–105.
- [9] C. Wang, R. Sun, R. Huang, H. Wang, Superior Fenton-like degradation of tetracycline by iron loaded graphitic carbon derived from microplastics: synthesis, catalytic performance, and mechanism, *Sep. Purif. Technol.*, 270 (2021) 118773, doi: 10.1016/j.seppur.2021.118773.
- [10] M. Aram, M. Farhadian, A.R.S. Nazar, S. Tangestaninejad, P. Eskandari, B.-H. Jeon, Metronidazole and cephalexin degradation by using of urea/ $\text{TiO}_2/\text{ZnFe}_2\text{O}_4/\text{clinoptilolite}$  catalyst under visible-light irradiation and ozone injection, *J. Mol. Liq.*, 304 (2020) 112764, doi: 10.1016/j.molliq.2020.112764.
- [11] Z. He, X. Wang, Y. Luo, Y. Zhu, X. Lai, J. Shang, J. Chen, Q. Liao, Effects of suspended particulate matter from natural lakes in conjunction with coagulation to tetracycline removal from water, *Chemosphere*, 277 (2021) 130327, doi: 10.1016/j.chemosphere.2021.130327.
- [12] M. Farzadkia, E. Bazrafshan, A. Esrafil, J.-K. Yang, M. Shirzad-Siboni, Photocatalytic degradation of metronidazole with illuminated  $\text{TiO}_2$  nanoparticles, *J. Environ. Health Sci. Eng.*, 13 (2015) 1–8.

- [13] N. Nasseh, B. Barikbin, L. Taghavi, M.A. Nasser, Adsorption of metronidazole antibiotic using a new magnetic nanocomposite from simulated wastewater (isotherm, kinetic and thermodynamic studies), *Composites, Part B*, 159 (2019) 146–156.
- [14] M. Yuan, C. Li, B. Zhang, J. Wang, J. Zhu, J. Ji, Y. Ma, A mild and one-pot method to activate lignin-derived biomass by using boric acid for aqueous tetracycline antibiotics removal in water, *Chemosphere*, 280 (2021) 130877, doi: 10.1016/j.chemosphere.2021.130877.
- [15] S. Liu, M. Pan, Z. Feng, Y. Qin, Y. Wang, L. Tan, T. Sun, Ultra-high adsorption of tetracycline antibiotics on garlic skin-derived porous biomass carbon with high surface area, *New J. Chem.*, 44 (2020) 1097–1106.
- [16] O. Qafoku, C.I. Pearce, A. Neumann, L. Kovarik, M. Zhu, E.S. Ilton, M.E. Bowden, C.T. Resch, B.W. Arey, E. Arenholz, Tc(VII) and Cr(VI) interaction with naturally reduced ferruginous smectite from a redox transition zone, *Environ. Sci. Technol.*, 51 (2017) 9042–9052.
- [17] C.H. Nguyen, C.-C. Fu, D.-Y. Kao, T.T. Van Tran, R.-S. Juang, Adsorption removal of tetracycline from water using poly(vinylidene fluoride)/polyaniline-montmorillonite mixed matrix membranes, *J. Taiwan Inst. Chem. Eng.*, 112 (2020) 259–270.
- [18] S. Guo, W. Yang, L. You, J. Li, J. Chen, K. Zhou, Simultaneous reduction of Cr(VI) and degradation of tetracycline hydrochloride by a novel iron-modified rectorite composite through heterogeneous photo-Fenton processes, *Chem. Eng. J.*, 393 (2020) 124758, doi: 10.1016/j.cej.2020.124758.
- [19] Y. Shi, Z. Yang, B. Wang, H. An, Z. Chen, H. Cui, Adsorption and photocatalytic degradation of tetracycline hydrochloride using a palygorskite-supported  $\text{Cu}_2\text{O}-\text{TiO}_2$  composite, *Appl. Clay Sci.*, 119 (2016) 311–320.
- [20] X. Tang, Y. Huang, Q. He, Y. Wang, H. Zheng, Y. Hu, Adsorption of tetracycline antibiotics by nitrilotriacetic acid modified magnetic chitosan-based microspheres from aqueous solutions, *Environ. Technol. Innovation*, 24 (2021) 101895, doi: 10.1016/j.eti.2021.101895.
- [21] M. Cao, X. Liu, W. Wang, M. Gao, H. Yang, Bifunctional two-dimensional copper-aluminum modified filter paper composite for efficient tetracycline removal: synergy of adsorption and reusability by degradation, *Chemosphere*, 287 (2022) 132031, doi: 10.1016/j.chemosphere.2021.132031.
- [22] K. Khaledi, G.M. Valdes Labrada, J. Soltan, B. Predicala, M. Nemati, Adsorptive removal of tetracycline and lincomycin from contaminated water using magnetized activated carbon, *J. Environ. Chem. Eng.*, 9 (2021) 105998, doi: 10.1016/j.jece.2021.105998.
- [23] C. Chen, X. Feng, S. Yao, Ionic liquid-multi walled carbon nanotubes composite tablet for continuous adsorption of tetracyclines and heavy metals, *J. Cleaner Prod.*, 286 (2021) 124937, doi: 10.1016/j.jclepro.2020.124937.
- [24] N. Nasseh, F.S. Arghavan, N. Daglioglu, A. Asadi, Fabrication of novel magnetic  $\text{CuS}/\text{Fe}_3\text{O}_4/\text{GO}$  nanocomposite for organic pollutant degradation under visible light irradiation, *Environ. Sci. Pollut. Res.*, 28 (2021) 19222–19233.
- [25] D. Mohan, A. Sarswat, V.K. Singh, M. Alexandre-Franco, C.U. Pittman Jr., Development of magnetic activated carbon from almond shells for trinitrophenol removal from water, *Chem. Eng. J.*, 172 (2011) 1111–1125.
- [26] Q. Liu, Y. Zheng, L. Zhong, X. Cheng, Removal of tetracycline from aqueous solution by a  $\text{Fe}_3\text{O}_4$  incorporated PAN electrospun nanofiber mat, *J. Environ. Sci. (China)*, 28 (2015) 29–36.
- [27] B. Kakavandi, A. Jonidi, R. Rezaei, S. Nasser, A. Ameri, A. Esrafily, Synthesis and properties of  $\text{Fe}_3\text{O}_4$ -activated carbon magnetic nanoparticles for removal of aniline from aqueous solution: equilibrium, kinetic and thermodynamic studies, *Iran. J. Environ. Health Sci. Eng.*, 10 (2013) 1–9, doi: 10.1186/1735-2746-10-19.
- [28] N. Nasseh, L. Taghavi, B. Barikbin, M.A. Nasser, Synthesis and characterizations of a novel  $\text{FeNi}_3/\text{SiO}_2/\text{CuS}$  magnetic nanocomposite for photocatalytic degradation of tetracycline in simulated wastewater, *J. Cleaner Prod.*, 179 (2018) 42–54.
- [29] D. Ayodhya, G. Veerabhadram, Facile fabrication, characterization and efficient photocatalytic activity of surfactant free ZnS, CdS and CuS nanoparticles, *J. Sci.: Adv. Mater. Devices*, 4 (2019) 381–391.
- [30] F. Mbarki, T. Selmi, A. Kesraoui, M. Seffen, Low-cost activated carbon preparation from corn stigmata fibers chemically activated using  $\text{H}_3\text{PO}_4$ ,  $\text{ZnCl}_2$  and KOH: study of methylene blue adsorption, stochastic isotherm and fractal kinetic, *Ind. Crops Prod.*, 178 (2022) 114546, doi: 10.1016/j.indcrop.2022.114546.
- [31] M. Wei, F. Marrakchi, C. Yuan, X. Cheng, D. Jiang, F.F. Zafar, Y. Fu, S. Wang, Adsorption modeling, thermodynamics, and DFT simulation of tetracycline onto mesoporous and high-surface-area NaOH-activated macroalgae carbon, *J. Hazard. Mater.*, 425 (2022) 127887, doi: 10.1016/j.jhazmat.2021.127887.
- [32] I. Özüdoğru, Z. Yigit Avdan, S. Balbay, A novel carbon-based material recycled from end-of-life tires (ELTs) for separation of organic dyes to understand kinetic and isotherm behavior, *Sep. Sci. Technol.*, 57 (2022) 2024–2040.
- [33] S. Kim, F. Gholamirad, M. Yu, C.M. Park, A. Jang, M. Jang, N. Taheri-Qazvini, Y. Yoon, Enhanced adsorption performance for selected pharmaceutical compounds by sonicated  $\text{Ti}_3\text{C}_2\text{T}_x$  MXene, *Chem. Eng. J.*, 406 (2021) 126789, doi: 10.1016/j.cej.2020.126789.
- [34] N. Nasseh, L. Taghavi, B. Barikbin, A.R. Harifi-Mood, The removal of Cr(VI) from aqueous solution by almond green hull waste material: kinetic and equilibrium studies, *J. Water Reuse Desal.*, 7 (2016) 449–460.
- [35] N. Nasseh, R. Khosravi, G.A. Rumman, M. Ghadirian, H. Eslami, M. Khoshnamvand, T.J. Al-Musawi, A. Khosravi, Adsorption of Cr(VI) ions onto powdered activated carbon synthesized from *Peganum harmala* seeds by ultrasonic waves activation, *Environ. Technol. Innovation*, 21 (2021) 101277, doi: 10.1016/j.eti.2020.101277.
- [36] L.R. de Carvalho Costa, L. de Moraes Ribeiro, G.E.N. Hidalgo, L.A. Féris, Evaluation of efficiency and capacity of thermal, chemical and ultrasonic regeneration of tetracycline exhausted activated carbon, *Environ. Technol.*, 43 (2022) 907–917.
- [37] N. Nasseh, R. Khosravi, N.S. Mazari Moghaddam, S. Rezaia, Effect of  $\text{UV}_c$  and  $\text{UV}_A$  photocatalytic processes on tetracycline removal using CuS-coated magnetic activated carbon nanocomposite: a comparative study, *Int. J. Environ. Res. Public Health*, 18 (2021) 11163, doi: 10.3390/ijerph182111163.
- [38] S. Suganya, Influence of ultrasonic waves on preparation of active carbon from coffee waste for the reclamation of effluents containing Cr(VI) ions, *J. Ind. Eng. Chem.*, 60 (2018) 418–430.
- [39] N. Mohammadi, A. Allahresani, A. Naghizadeh, Novel fibrous silica-copper sulfide nanocomposite (KCC1-CuS): synthesis and enhanced photocatalytic degradation of humic acid, (2021), doi: 10.21203/rs.3.rs-157129/v1.
- [40] Q. Liu, L.-B. Zhong, Q.-B. Zhao, C. Frear, Y.-M. Zheng, Synthesis of  $\text{Fe}_3\text{O}_4$ /polyacrylonitrile composite electrospun nanofiber mat for effective adsorption of tetracycline, *ACS Appl. Mater. Interfaces*, 7 (2015) 14573–14583.
- [41] Y. Wang, H. Zhang, J. Zhang, C. Lu, Q. Huang, J. Wu, F. Liu, Degradation of tetracycline in aqueous media by ozonation in an internal loop-lift reactor, *J. Hazard. Mater.*, 192 (2011) 35–43.
- [42] M. Ahmed, M.A. Islam, M. Asif, B. Hameed, Human hair-derived high surface area porous carbon material for the adsorption isotherm and kinetics of tetracycline antibiotics, *Bioresour. Technol.*, 243 (2017) 778–784.
- [43] Y. Chen, F. Wang, L. Duan, H. Yang, J. Gao, Tetracycline adsorption onto rice husk ash, an agricultural waste: its kinetic and thermodynamic studies, *J. Mol. Liq.*, 222 (2016) 487–494.
- [44] D. Fernández-Calviño, A. Bermúdez-Couso, M. Arias-Estévez, J.C. Nóvoa-Muñoz, M.J. Fernández-Sanjurjo, E. Álvarez-Rodríguez, A. Núñez-Delgado, Kinetics of tetracycline, oxytetracycline, and chlortetracycline adsorption and desorption on two acid soils, *Environ. Sci. Pollut. Res.*, 22 (2015) 425–433.
- [45] N. Samira, H. Mohsen, A. Vali, R. Omid, F. Mehdi, F. Mohammadi-moghadam, N. Heshmatollah, B. Goudarzi, D. Kavooos, Preparation, characterization and Cr(VI) adsorption evaluation of NaOH-activated carbon produced from Date

- Press Cake; an agro-industrial waste, *Bioresour. Technol.*, 258 (2018) 48–56.
- [46] X. Zhang, X. Lin, Y. He, Y. Chen, X. Luo, R. Shang, Study on adsorption of tetracycline by Cu-immobilized alginate adsorbent from water environment, *Int. J. Biol. Macromol.*, 124 (2019) 418–428.
- [47] Z. Zhang, K. Sun, B. Gao, G. Zhang, X. Liu, Y. Zhao, Adsorption of tetracycline on soil and sediment: effects of pH and the presence of Cu(II), *J. Hazard. Mater.*, 190 (2011) 856–862.
- [48] S.M. Al-Jubouri, S.M. Holmes, Immobilization of cobalt ions using hierarchically porous 4A zeolite-based carbon composites: ion-exchange and solidification, *J. Water Process Eng.*, 33 (2020) 101059, doi: 10.1016/j.jwpe.2019.101059.
- [49] P. Chitra, A. Muthusamy, R. Jayaprakash, E.R. Kumar, Effect of ultrasonication on particle size and magnetic properties of polyaniline NiCoFe<sub>2</sub>O<sub>4</sub> nanocomposites, *J. Magn. Magn. Mater.*, 366 (2014) 55–63.
- [50] M. Kamranifar, A. Allahresani, A. Naghizadeh, Synthesis and characterizations of a novel CoFe<sub>2</sub>O<sub>4</sub>@CuS magnetic nanocomposite and investigation of its efficiency for photocatalytic degradation of penicillin G antibiotic in simulated wastewater, *J. Hazard. Mater.*, 366 (2019) 545–555.
- [51] C. Anyika, N.A.M. Asri, Z.A. Majid, A. Yahya, J. Jaafar, Synthesis and characterization of magnetic activated carbon developed from palm kernel shells, *Nanotechnol. Environ. Eng.*, 2 (2017) 1–25.
- [52] T. Depci, Comparison of activated carbon and iron impregnated activated carbon derived from Gölbaşı lignite to remove cyanide from water, *Chem. Eng. J.*, 181 (2012) 467–478.
- [53] S.M. Mirsoleimani-Azizi, P. Setoodeh, S. Zeinali, M.R. Rahimpour, Tetracycline antibiotic removal from aqueous solutions by MOF-5: adsorption isotherm, kinetic and thermodynamic studies, *J. Environ. Chem. Eng.*, 6 (2018) 6118–6130.
- [54] J.H. Kwon, L.D. Wilson, R. Sammynaiken, Synthesis and characterization of magnetite and activated carbon binary composites, *Synth. Met.*, 197 (2014) 8–17.
- [55] S.C. Rodrigues, M.C. Silva, J.A. Torres, M.L. Bianchi, Use of magnetic activated carbon in a solid phase extraction procedure for analysis of 2,4-dichlorophenol in water samples, *Water Air Soil Pollut.*, 231 (2020) 1–13.
- [56] K.K. Hammud, N.M. Imra, M.H. Khalil, N.A.H. Akosh, F.M. Hamza, D.E. Zanad, Preparation and characterization of magnetic activated carbon as non-hemolytic material, *AIP Conf. Proc.*, 2372 (2021) 130021, doi: 10.1063/5.0065417.
- [57] T. Ahamad, Mu. Naushad, T. Al-Shahrani, N. Al-Hokbany, S.M. Alshehri, Preparation of chitosan based magnetic nanocomposite for tetracycline adsorption: kinetic and thermodynamic studies, *Int. J. Biol. Macromol.*, 147 (2020) 258–267.
- [58] H. Liu, X. Wang, G. Zhai, J. Zhang, C. Zhang, N. Bao, C. Cheng, Preparation of activated carbon from lotus stalks with the mixture of phosphoric acid and pentaerythritol impregnation and its application for Ni(II) sorption, *Chem. Eng. J.*, 209 (2012) 155–162.
- [59] J.W. Brown, P.S. Ramesh, D. Geetha, Fabrication of mesoporous iron (Fe) doped copper sulfide (CuS) nanocomposite in the presence of a cationic surfactant via mild hydrothermal method for supercapacitors, *Mater. Res. Express*, 5 (2018) 024007, doi: 10.1088/2053-1591/aaad55.
- [60] N. Nasseh, B. Barikbin, L. Taghavi, Photocatalytic degradation of tetracycline hydrochloride by FeNi<sub>2</sub>/SiO<sub>2</sub>/CuS magnetic nanocomposite under simulated solar irradiation: efficiency, stability, kinetic and pathway study, *Environ. Technol. Innovation*, 20 (2020) 101035, doi: 10.1016/j.eti.2020.101035.
- [61] A. Dehghan, M.H. Dehghani, R. Nabizadeh, N. Ramezani, M. Alimohammadi, A.A. Najafpoor, Adsorption and visible-light photocatalytic degradation of tetracycline hydrochloride from aqueous solutions using 3D hierarchical mesoporous BiOI: synthesis and characterization, process optimization, adsorption and degradation modeling, *Chem. Eng. Res. Des.*, 129 (2018) 217–230.
- [62] M. Erşan, E. Bağda, E. Bağda, Investigation of kinetic and thermodynamic characteristics of removal of tetracycline with sponge like, tannin based cryogels, *Colloids Surf., B*, 104 (2013) 75–82.
- [63] Y. Gao, Y. Li, L. Zhang, H. Huang, J. Hu, S.M. Shah, X. Su, Adsorption and removal of tetracycline antibiotics from aqueous solution by graphene oxide, *J. Colloid Interface Sci.*, 368 (2012) 540–546.
- [64] H. Liu, G. Xu, G. Li, Preparation of porous biochar based on pharmaceutical sludge activated by NaOH and its application in the adsorption of tetracycline, *J. Colloid Interface Sci.*, 587 (2021) 271–278.
- [65] H. Wu, H. Xie, G. He, Y. Guan, Y. Zhang, Effects of the pH and anions on the adsorption of tetracycline on iron-montmorillonite, *Appl. Clay Sci.*, 119 (2016) 161–169.
- [66] M.H. Marzbali, M. Esmaili, H. Abolghasemi, M.H. Marzbali, Tetracycline adsorption by H<sub>3</sub>PO<sub>4</sub>-activated carbon produced from apricot nut shells: a batch study, *Process Saf. Environ. Prot.*, 102 (2016) 700–709.
- [67] W.-R. Chen, C.-H. Huang, Transformation kinetics and pathways of tetracycline antibiotics with manganese oxide, *Environ. Pollut.*, 159 (2011) 1092–1100.
- [68] Y. Zhao, J. Geng, X. Wang, X. Gu, S. Gao, Tetracycline adsorption on kaolinite: pH, metal cations and humic acid effects, *Ecotoxicology*, 20 (2011) 1141–1147.
- [69] P. Liu, W.-J. Liu, H. Jiang, J.-J. Chen, W.-W. Li, H.-Q. Yu, Modification of bio-char derived from fast pyrolysis of biomass and its application in removal of tetracycline from aqueous solution, *Bioresour. Technol.*, 121 (2012) 235–240.
- [70] G. Yang, Q. Gao, S. Yang, S. Yin, X. Cai, X. Yu, S. Zhang, Y. Fang, Strong adsorption of tetracycline hydrochloride on magnetic carbon-coated cobalt oxide nanoparticles, *Chemosphere*, 239 (2020) 124831, doi: 10.1016/j.chemosphere.2019.124831.
- [71] M.M. Ali, M. Ahmed, B. Hameed, NaY zeolite from wheat (*Triticum aestivum* L.) straw ash used for the adsorption of tetracycline, *J. Cleaner Prod.*, 172 (2018) 602–608.
- [72] X. Zhu, Y. Liu, C. Zhou, G. Luo, S. Zhang, J. Chen, A novel porous carbon derived from hydrothermal carbon for efficient adsorption of tetracycline, *Carbon*, 77 (2014) 627–636.
- [73] A.R. Kaveeshwar, S.K. Ponnusamy, E.D. Revellame, D.D. Gang, M.E. Zappi, R. Subramaniam, Pecan shell based activated carbon for removal of iron(II) from fracking wastewater: adsorption kinetics, isotherm and thermodynamic studies, *Process Saf. Environ. Prot.*, 114 (2018) 107–122.
- [74] A.F. Alkaim, Z. Sadik, D.K. Mahdi, S.M. Alshrefi, A.M. Al-Sammaraie, F.M. Alamgir, P.M. Singh, A.M. Aljeboree, Preparation, structure and adsorption properties of synthesized multiwall carbon nanotubes for highly effective removal of maxilon blue dye, *Korean J. Chem. Eng.*, 32 (2015) 2456–2462.
- [75] M.K. Aroua, S. Leong, L. Teo, C.Y. Yin, W.M.A.W. Daud, Real-time determination of kinetics of adsorption of lead(II) onto palm shell-based activated carbon using ion selective electrode, *Bioresour. Technol.*, 99 (2008) 5786–5792.
- [76] J. Chang, Z. Shen, X. Hu, E. Schulman, C. Cui, Q. Guo, H. Tian, Adsorption of tetracycline by shrimp shell waste from aqueous solutions: adsorption isotherm, kinetics modeling, and mechanism, *ACS Omega*, 5 (2020) 3467–3477.
- [77] M. Fazlzadeh, R. Khosravi, A. Zarei, Green synthesis of zinc oxide nanoparticles using *Peganum harmala* seed extract, and loaded on *Peganum harmala* seed powdered activated carbon as new adsorbent for removal of Cr(VI) from aqueous solution, *Ecol. Eng.*, 103 (2017) 180–190.
- [78] G. Kirova, Z. Velkova, M. Stoytcheva, V. Gochev, Tetracycline removal from model aqueous solutions by pretreated waste *Streptomyces fradiae* biomass, *Biotechnol. Biotechnol. Equip.*, 35 (2021) 953–963.
- [79] A. Nasiri, M. Malakootian, M.A. Shiri, G. Yazdanpanah, M. Nozari, CoFe<sub>2</sub>O<sub>4</sub>@methylcellulose synthesized as a new magnetic nanocomposite to tetracycline adsorption: modeling, analysis, and optimization by response surface methodology, *J. Polym. Res.*, 28 (2021) 1–23.
- [80] D. Xu, Y. Gao, Z. Lin, W. Gao, H. Zhang, K. Karnowo, X. Hu, H. Sun, S.S.A. Syed-Hassan, S. Zhang, Application of biochar derived from pyrolysis of waste fiberboard on tetracycline adsorption in aqueous solution, *Front. Chem.*, 7 (2020) 943, doi: 10.3389/fchem.2019.00943.

- [81] M. Rathod, S. Haldar, S. Basha, Nanocrystalline cellulose for removal of tetracycline hydrochloride from water via biosorption: equilibrium, kinetic and thermodynamic studies, *Ecol. Eng.*, 84 (2015) 240–249.
- [82] K. Li, F. Ji, Y. Liu, Z. Tong, X. Zhan, Z. Hu, Adsorption removal of tetracycline from aqueous solution by anaerobic granular sludge: equilibrium and kinetic studies, *Water Sci. Technol.*, 67 (2013) 1490–1496.
- [83] A.A. Mohammed, S.L. Kareem, Adsorption of tetracycline from wastewater by using Pistachio shell coated with ZnO nanoparticles: equilibrium, kinetic and isotherm studies, *Alexandria Eng. J.*, 58 (2019) 917–928.
- [84] H. Zhu, T. Chen, J. Liu, D. Li, Adsorption of tetracycline antibiotics from an aqueous solution onto graphene oxide/calcium alginate composite fibers, *RSC Adv.*, 8 (2018) 2616–2621.
- [85] D. Balarak, F.K. Mostafapour, A. Joghataei, Experimental and kinetic studies on penicillin G adsorption by *Lemna minor*, *J. Pharm. Res. Int.*, 9 (2016) 1–10.
- [86] X. Cheng, H. Hou, R. Li, C. Zheng, H. Liu, Adsorption behavior of tetracycline on the soil and molecular insight into the effect of dissolved organic matter on the adsorption, *J. Soils Sediments*, 20 (2020) 1846–1857.
- [87] R. Zhao, T. Ma, S. Zhao, H. Rong, Y. Tian, G. Zhu, Uniform and stable immobilization of metal-organic frameworks into chitosan matrix for enhanced tetracycline removal from water, *Chem. Eng. J.*, 382 (2020) 122893, doi: 10.1016/j.cej.2019.122893.

## Supporting information

### S1: Isotherm models

To study the adsorption isotherm mechanisms, experimental data were analyzed using the Langmuir, Freundlich, and Temkin isotherm equations.

#### S1.1. Langmuir isotherm equations

The Langmuir model is based on monolayer adsorption. Adsorption on the sorbent has a limited number of valid adsorption sites [Eq. (S1)]. The necessary parameter for the Langmuir isotherm model that identifies the isotherm type is the  $R_l$  constant that is also known as the equilibrium constant [Eq. (S2)] [S1].

$$q_e = \frac{q_m K_L C_e}{1 + K_L C_e} \quad (\text{S1})$$

$$R_l = \frac{1}{1 + bC_0} \quad (\text{S2})$$

where  $q_e$  (mg/g) is the quantity of contaminant adsorbed per gram,  $q_m$  (mg/g) is the maximum adsorption capacity,  $K_L$  (L/mg) is the Langmuir constant,  $C_e$  (mg/L) is the concentration of the adsorbed contaminant at equilibrium,  $b = K_L$  (L/mg), and  $C_0$  (mg/g) is the initial concentration of the adsorbate.  $R_l = 0$  indicates an irreversible isotherm,  $0 < R_l < 1$  represents an optimal isotherm,  $R_l = 1$  is a linear isotherm, and  $R_l > 1$  indicates that the isotherm is suboptimal [S2].

#### S1.2. Freundlich isotherm equations

The Freundlich model [Eq. (S3)] is based on multi-layered adsorption, heterogeneous adsorption places with unequal energy, and the suitability of the adsorbent [S2,S3].

$$q_e = K_f C_e^{1/n} \quad (\text{S3})$$

where  $C_e$  (mg/L) is the concentration of the adsorbed contaminant at equilibrium,  $K_f$  ( $[\text{mg/g}] \cdot [\text{L/mg}]^{1/n}$ ) is the Freundlich constant that indicates the adsorption capacity, and  $n$  is the Freundlich constant and a measure of adsorption linearity. When the  $K_f$  value is increased, the substance adsorption capacity is also increased. Additionally, when the value of  $n$  is between 1 and 10, the adsorption process is suitable. If  $n$  is close to 1, the heterogeneity of the surface is less significant, and if this value is close to 10, it becomes more important.

#### S1.3. Temkin isotherm equations

The Temkin isotherm [Eq. (S4)] adsorption model was used to evaluate the potential of the adsorbent for the adsorbate. This isotherm considers the adsorbent–adsorbate interactions. Additionally, in this model extremely low and high concentrations of adsorbate were neglected [S4].

$$q_e = \frac{RT}{B_t} \ln(K_t C_e) \quad (\text{S4})$$

where  $R$  (8.314 J/mol·K) is the universal gas constant,  $T$  (298 K) is the absolute temperature in Kelvin,  $K_t$  (L/g) is the Temkin isotherm constant, and  $B_t$  (J/mol) is the Temkin constant related to the adsorption heat.

### S2: Kinetic models

For the kinetic analysis of the adsorption rate, two common pseudo-first-order [Eq. (S5)] and pseudo-second-order [Eq. (S6)] models were used to analyze the equilibrium data as follows. The coefficient of determination ( $R^2$ ) is a measure of consistency between the experimental data and two proposed models [S3–S5].

$$q_t = q_e [1 - \exp(-K_1 t)]; h_0 = k_1 q_e \quad (\text{S5})$$

$$q_t = \frac{K_2 q_e^2 t}{1 + K_2 q_e t}; h_0 = k_2 q_e^2 \quad (\text{S6})$$

where  $k_1$  ( $\text{min}^{-1}$ ) is the rate constant of the Lagergren pseudo-first-order model,  $k_2$  (g/mg·min) is the rate constant of the pseudo-second-order model,  $h_0$  is the initial adsorption rate,  $q_t$  (mg/g) is the adsorbed amount at any given time, and  $q_e$  (mg/g) is the adsorbed amount at equilibrium.

### S3: Thermodynamic calculation of the adsorption process

Eqs. (S7) and (S8) were used for the thermodynamic analysis of tetracycline using the magnetic MAC/CuS nanocomposites.

$$\Delta G^\circ = -RT \ln k_d \quad (\text{S7})$$

$$\ln k_d = \frac{\Delta S^\circ}{R} - \frac{\Delta H^\circ}{RT} \quad (\text{S8})$$

In Eq. (S7),  $\Delta G^\circ$  is the Gibbs free energy,  $R$  is the (8.314 J/mol·K) gas constant,  $T$  is temperature in K, and  $k_d$  is the thermodynamic equilibrium constant. In Eq. (S8),  $\Delta S^\circ$  is the standard entropy (J/mol·K), and  $\Delta H^\circ$  is the standard enthalpy change (kJ/mol). After calculating the thermodynamic equilibrium constant and the corresponding free energy at various temperatures,  $\ln k_d$  was plotted against  $1/T$ . The slope and intercept were used to obtain  $\Delta S^\circ$  and  $\Delta H^\circ$  values, respectively [S6].

## References

- [S1] N. Samira, H. Mohsen, A. Vali, R. Omid, F. Mehdi, F. Mohammadi-moghadam, N. Heshmatollah, B. Goudarzi, D. Kavos, Preparation, characterization and Cr(VI) adsorption evaluation of NaOH-activated carbon produced from Date Press Cake; an agro-industrial waste, *Bioresour. Technol.*, 258 (2018) 48–56.
- [S2] X. Zhang, X. Lin, Y. He, Y. Chen, X. Luo, R. Shang, Study on adsorption of tetracycline by Cu-immobilized alginate adsorbent from water environment, *Int. J. Biol. Macromol.*, 124 (2019) 418–428.
- [S3] N. Nasseh, L. Taghavi, B. Barikbin, A.R. Harifi-Mood, The removal of Cr(VI) from aqueous solution by almond green hull waste material: kinetic and equilibrium studies, *J. Water Reuse Desal.*, 7 (2016) 449–460.
- [S4] N. Nasseh, R. Khosravi, G.A. Rumman, M. Ghadirian, H. Eslami, M. Khoshnamvand, T.J. Al-Musawi, A. Khosravi, Adsorption of Cr(VI) ions onto powdered activated carbon synthesized from *Peganum harmala* seeds by ultrasonic waves activation, *Environ. Technol. Innovation*, 21 (2021) 101277, doi: 10.1016/j.eti.2020.101277.
- [S5] Y. Chen, F. Wang, L. Duan, H. Yang, J. Gao, Tetracycline adsorption onto rice husk ash, an agricultural waste: its kinetic and thermodynamic studies, *J. Mol. Liq.*, 222 (2016) 487–494.
- [S6] D. Fernández-Calviño, A. Bermúdez-Couso, M. Arias-Estévez, J.C. Nóvoa-Muñoz, M.J. Fernández-Sanjurjo, E. Álvarez-Rodríguez, A. Núñez-Delgado, Kinetics of tetracycline, oxytetracycline, and chlortetracycline adsorption and desorption on two acid soils, *Environ. Sci. Pollut. Res.*, 22 (2015) 425–433.